Time-resolved spectral characterization of ring cavity surface emitting and ridge-type distributed feedback quantum cascade lasers by step-scan FT-IR spectroscopy

Markus Brandstetter,[1,4] Andreas Genner,[1,4] Clemens Schwarzer,[2] Elvis Mujagic,[3] Gottfried Strasser,[2] and Bernhard Lendl[1,*]

[1]*Institute of Chemical Technologies and Analytics, Vienna University of Technology, Getreidemarkt 9 /164AC, 1060 Vienna, Austria*
[2]*Institute for Solid State Electronics, Vienna University of Technology, Floragasse 7, 1040 Vienna, Austria*
[3]*Siemens Building Technologies,Siemens Switzerland, 6300 Zug, Switzerland*
[4]*These authors contributed equally to this work*
[*]*bernhard.lendl@tuwien.ac.at*

Abstract: We present the time-resolved comparison of pulsed 2nd order ring cavity surface emitting (RCSE) quantum cascade lasers (QCLs) and pulsed 1st order ridge-type distributed feedback (DFB) QCLs using a step-scan Fourier transform infrared (FT-IR) spectrometer. Laser devices were part of QCL arrays and fabricated from the same laser material. Required grating periods were adjusted to account for the grating order. The step-scan technique provided a spectral resolution of 0.1 cm^{-1} and a time resolution of 2 ns. As a result, it was possible to gain information about the tuning behavior and potential mode-hops of the investigated lasers. Different cavity-lengths were compared, including 0.9 mm and 3.2 mm long ridge-type and 0.97 mm (circumference) ring-type cavities. RCSE QCLs were found to have improved emission properties in terms of line-stability, tuning rate and maximum emission time compared to ridge-type lasers.

OCIS codes: (140.0140) Lasers and laser optics; (300.0300) Spectroscopy.

References

1. J. Faist, F. Capasso, D. L. Sivco, C. Sirtori, A. L. Hutchinson, and A. Y. Cho, "Quantum cascade laser," Science **264**(5158), 553–556 (1994).
2. G. P. Luo, C. Peng, H. Q. Le, S. S. Pei, W.-Y. Hwang, B. Ishaug, J. Um, J. N. Baillargeon, and C.-H. Lin, "Grating-tuned external-cavity quantum-cascade semiconductor lasers," Appl. Phys. Lett. **78**(19), 2834–2836 (2001).
3. J. Faist, C. Gmachl, F. Capasso, C. Sirtori, D. L. Sivco, J. N. Baillargeon, and A. Y. Cho, "Distributed feedback quantum cascade lasers," Appl. Phys. Lett. **70**(20), 2670–2672 (1997).
4. G. Hancock, "Applications of midinfrared quantum cascade lasers to spectroscopy," Opt. Eng. **49**(11), 111121 (2010).
5. R. F. Curl, F. Capasso, C. Gmachl, A. Kosterev, B. McManus, R. Lewicki, M. Pusharsky, G. Wysocki, and F. K. Tittel, "Quantum cascade lasers in chemical physics," Chem. Phys. Lett. **487**(1–3), 1–18 (2010).
6. J. B. McManus, M. S. Zahniser, D. D. Nelson, Jr., J. H. Shorter, S. Herndon, E. Wood, and R. Wehr, "Application of quantum cascade lasers to high-precision atmospheric trace gas measurements," Opt. Eng. **49**(11), 111124 (2010).
7. K. Namjou, S. Cai, E. A. Whittaker, J. Faist, C. Gmachl, F. Capasso, D. L. Sivco, and A. Y. Cho, "Sensitive absorption spectroscopy with a room-temperature distributed-feedback quantum-cascade laser," Opt. Lett. **23**(3), 219–221 (1998).
8. M. T. McCulloch, E. L. Normand, N. Langford, G. Duxbury, and D. A. Newnham, "Highly sensitive detection of trace gases using the time-resolved frequency downchirp from pulsed quantum-cascade lasers," J. Opt. Soc. Am. B **20**(8), 1761–1768 (2003).
9. C. Pflügl, W. Schrenk, S. Anders, and G. Strasser, "Spectral dynamics of distributed feedback quantum cascade lasers," Semicond. Sci. Technol. **19**(4), S336–S338 (2004).

#200147 - $15.00 USD Received 29 Oct 2013; revised 2 Jan 2014; accepted 6 Jan 2014; published 30 Jan 2014

10. T. J. Johnson, A. Simon, J. M. Weil, and G. W. Harris, "Applications of time-resolved step-scan and rapid-scan FT-IR spectroscopy : dynamics from ten seconds to ten nanoseconds," Appl. Spectrosc. **47**(9), 1376–1381 (1993).
11. W. Uhmann, A. Becker, C. Taran, and F. Siebert, "Time-resolved FT-IR absorption spectroscopy using a step-scan interferometer," Appl. Spectrosc. **45**(3), 390–397 (1991).
12. J.-M. Melkonian, J. Petit, M. Raybaut, A. Godard, and M. Lefebvre, "Time-resolved spectral characterization of a pulsed external-cavity quantum cascade laser," in *Conference on Lasers and Electro-Optics 2012* (OSA, 2012), paper CF2K.4.
13. B. Hinkov, Q. Yang, F. Fuchs, W. Bronner, K. Köhler, and J. Wagner, "Time-resolved characterization of external-cavity quantum-cascade lasers," Appl. Phys. Lett. **94**(22), 221105 (2009).
14. M. Brandstetter and B. Lendl, "Tunable mid-infrared lasers in physical chemosensors towards the detection of physiologically relevant parameters in biofluids," Sens. Actuators B Chem. **170**, 189–195 (2012).
15. Z. Liu, D. Wasserman, S. S. Howard, A. J. Hoffman, C. Gmachl, X. Wang, T. Tanbun-Ek, L. Cheng, and F. S. Choa, "Room-temperature continuous-wave quantum cascade lasers grown by MOCVD without lateral regrowth," IEEE Photonics Technol. Lett. **18**(12), 1347–1349 (2006).
16. E. Mujagić, S. Schartner, L. K. Hoffmann, W. Schrenk, M. P. Semtsiv, M. Wienold, W. T. Masselink, and G. Strasser, "Grating-coupled surface emitting quantum cascade ring lasers," Appl. Phys. Lett. **93**(1), 011108 (2008).
17. E. Mujagić, M. Nobile, H. Detz, W. Schrenk, J. Chen, C. Gmachl, and G. Strasser, "Ring cavity induced threshold reduction in single-mode surface emitting quantum cascade lasers," Appl. Phys. Lett. **96**(3), 031111 (2010).
18. H. Kogelnik and C. V. Shank, "Coupled-wave theory of distributed feedback lasers," J. Appl. Phys. **43**(5), 2327 (1972).
19. N. Finger and E. Gornik, "Analysis of metallized-grating coupled twin-waveguide structures," IEEE J. Quantum Electron. **35**(5), 832–843 (1999).
20. J. Buus, "Mode selectivity in DFB lasers with cleaved facets," Electron. Lett. **21**(5), 179–180 (1985).
21. H. K. Lee and J. S. Yu, "Thermal effects in quantum cascade lasers at λ~4.6 μm under pulsed and continuous-wave modes," Appl. Phys. B **106**(3), 619–627 (2011).
22. E. Mujagić, C. Schwarzer, Y. Yao, J. Chen, C. Gmachl, and G. Strasser, "Two-dimensional broadband distributed-feedback quantum cascade laser arrays," Appl. Phys. Lett. **98**(14), 141101 (2011).

1. Introduction

Over the last two decades Quantum Cascade Lasers (QCLs) developed from novel and high sophisticated lasers [1] to important light sources for use in mid-infrared (IR) spectroscopy. While in the beginning of their development only multi-mode emitting QCLs with a Fabry-Pérot (FP) cavity were available, technical improvements such as the external cavity (EC) [2] or the integration of a Bragg grating (distributed feedback - DFB) [3] enabled single mode emission. Consequently, this makes them well suited for gas phase spectroscopy of small molecules as the observed ro-vibrational absorption bands are typically sharp and highly resolved [4,5].

When designing a QCL based gas sensor, important parameters to be considered are the emission power, emitted wavelength and the operation mode (continuous wave - cw or pulsed) of the employed laser device. Sensors using QCLs in cw mode are well known to enable extremely low detection limits either by direct absorption and curve fitting [6] or by application of modulation techniques, such as wavelength modulation [7]. On the other hand, pulsed QCLs tune over several wavenumbers during a pulse due to internal Joule heating of the device. As it heats up during the pulse, the refractive index increases and simultaneously the laser device itself expands, leading to a red-shift of the emission frequency. In combination with a fast detector, multiple rotational-vibrational absorption bands of several analytes can be measured enabling simultaneous quantitative analysis of these compounds (intra-pulse technique) [8]. For that reason it is generally desirable to count with a large tuning range as this will increase the applicability of a given laser to different analytes. Hence, for gas sensor development a thorough spectroscopic characterization of the QC laser, particularly concerning its time-resolved tuning behavior is of importance. Basically, four different methods are available for that purpose: (i) the etalon, (ii) frequency upconversion (iii) FT-IR-spectrometer with gated signal acquisition [3,9], (iv) and the step-scan technique [10,11]. Since the etalon method is based on an FP interferometer, it is only applicable to single mode lasers as the resulting oscillating signal contains no absolute wavelength information and mode hops can only be detected by the phase shifts. Frequency upconversion requires non-linear optical crystals and a pump source to shift the mid-infrared QC laser

#200147 - $15.00 USD Received 29 Oct 2013; revised 2 Jan 2014; accepted 6 Jan 2014; published 30 Jan 2014

radiation up to near-infrared where it can subsequently be analyzed by a conventional optical spectrum analyzer [12]. Again, this method is not applicable to laser devices with broader spectral tuning ranges, as the bandwidth of the non-linear crystal can be limiting. More convenient and versatile approaches are the gated signal acquisition and step-scan FT-IR technique. Both were already successfully applied for the characterization of external cavity QCLs [13,14].

In this work we concentrated on time-resolved characterization of pulsed QCLs, namely standard ridge-type facet emitting and ring-type surface emitting DFB QCLs using the step scan FT-IR technique. The latter was chosen because it brings along some metrological and practical benefits as will be explained below.

2. Materials and methods

2.1 Laser material

The lasers used in this study were based on the material published in [15] and processed as described in [16]. The experimentally obtained temperature tuning rate was −0.085 cm^{-1}/K [17]. This rate is a combination of tuning due to an increase of the refractive index and a thermal expansion of the material which lies around −0.019 cm^{-1}/K (thermal expansion coefficient $\alpha = 4.6*10^{-6}$/K) for the present devices. Three different laser configurations were realized, including ring-cavity as well as a long and short ridge-type DFB QCLs. The RCSE QCL's grating period was 2.45 μm (2nd order) with 60 percent duty cycle, the waveguide width was 10 μm and the inner radius of the ring structure was 150 μm. For comparison, DFB lasers with a 1st order grating (1.225 μm) in ridge geometry were processed with a length of 0.9 (short DFB) and 3.2 mm (long DFB) and the same waveguide width of 10 μm. To achieve similar coupling strengths for the short DFB and second-order ring designs, the grating depths were adapted. A coupling strength κL of 1.6 was achieved with a 1.9 μm deep second order grating at the ring waveguide and a 0.7 μm deep first order grating at the ridge-type devices. Due to technological reasons, the grating depths at the long and the short ridge-type DFB laser are equal, leading to a slightly overcoupled grating at the long device (κL = 6.5). At such a device, the longitudinal mode intensity is more centred in the middle of the resonator reducing the influence of the facets [18].

To obtain information about the DFB coupling scheme, both waveguide structures were simulated [19]. For the first order grating a coupling constant $\kappa = (17.33 + 0.57i)$ cm^{-1} and for the second order structure a $\kappa = (13.6 + 9.07i)$ cm^{-1} was obtained. The small imaginary part for first order grating implies that these lasers are almost index coupled and the formation of a stop-band with a width of approximately 1.6 cm^{-1} can be expected. At the second order, complex coupled grating, the presence of loss-coupling leads to a robust operation of one distinctive DFB mode. From this simulation, also the waveguide losses are obtained. These are 16.9 cm^{-1} for the second order, and 7.03 cm^{-1} for the first order structure. The vertical extraction losses for the second order grating are 6.72 cm^{-1}.

Under ambient conditions (291 K), the emitted wavelength of the three different lasers was around 1282 cm^{-1}, determined by the Bragg grating's period. The devices were mounted on a Peltier cooling stage which allowed to adjust temperatures between 284 K and 296 K. A custom built laser driver was used to operate the QCLs at 10 kHz repetition rate with a pulse length of 2 μs. Table 1 summarizes the investigated QCL devices.

#200147 - $15.00 USD Received 29 Oct 2013; revised 2 Jan 2014; accepted 6 Jan 2014; published 30 Jan 2014

Table 1. Investigated QCL configurations of the same laser material. The waveguide width was the same for all devices (10 µm).

Laser configuration	Physical cavity length	Relevant cross section	Emission property	Form factor
Short DFB ridge	0.9 mm	0.009 mm^2	Facet emitter	
Long DFB ridge	3.2 mm	0.032 mm^2		
Ring-cavity surface emitting (RCSE)	0.97 mm	0.0097 mm^2	Surface emitter	

2.2 Time-resolved spectral characterization using the step-scan technique

Spectral characterization of the laser devices was performed with a Vertex 80v vacuum Fourier-transform infrared (FTIR) spectrometer (Bruker Optics GmbH, Germany) with a nominal maximum spectral resolution of 0.07 cm^{-1}. The spectrometer was equipped with a liquid-nitrogen cooled photovoltaic Mercury-Cadmimum-Telluride (MCT) infrared detector (Kolmar Technologies, USA) with a time constant of ~2 ns placed inside the spectrometer. Fourier transformation was performed with a Blackman-Harris-3-Term apodization function and the Mertz phase correction method (0.4 cm^{-1} phase resolution).

FTIR spectrometers are frequently employed for characterization of QCL devices using the rapid scan mode. Due to the low time resolution in the ms-range, this technique only allows to measure the envelope of the emission characteristic of the employed laser. A convenient way to obtain a more detailed information on the actual tuning behavior of the pulsed laser, with nanosecond time-resolution, is to make use of the step scan technique [10,11]. This technique can be used to study processes which can be repeatedly executed, a condition which is well met by pulsed quantum cascade lasers. The technique is based on a step-wise increase of the optical path difference of the interferometer of the spectrometer. At each step the change in intensity at the detector is recorded as a function of time. The time resolution hence only depends on the response time of the detector, the corresponding electronics (transient recorder) and the precision by which the laser can be operated. Signal alterations, as observed with boxcar gated signal acquisition due to the fast gating process, are avoided here [13]. Furthermore, spectral and time resolution are completely independent from each other. After having recorded the time dependent response for all required steps the data are re-ordered to assemble interferograms for each time slice. These interferograms are then Fourier transformed yielding the desired time resolved spectra. In this way high resolution can be maintained in both spectral and time domain. In addition to pulsed QCLs, cw operated QCLs can be characterized, too, given that some kind of repeated modulation is applied to the laser. The employed photovoltaic detector together with the transient recorder used (Spectrum GmbH, Germany) provided a maximum time resolution of 2 ns. Step-scan measurements at different laser currents were performed with a spectral resolution of 0.1 cm^{-1} and 2 ns time resolution.

Ridge-type DFB-QCLs had a much larger divergence (~60° full divergence) than ring-type DFB QCLs (~6° full divergence) [16]. In order to achieve comparable conditions for both laser types the emitted radiation was collimated with a 2 inch off-axis parabolic mirror (64 mm focal length) and coupled into the FTIR spectrometer using the port for external sources.

#200147 - $15.00 USD Received 29 Oct 2013; revised 2 Jan 2014; accepted 6 Jan 2014; published 30 Jan 2014

3. Results and discussion

3.1 Time-resolved vs. conventional non-time-resolved FT-IR spectroscopy

For a demonstrative comparison between these two characterization methods, a device which exhibits mode-hops was selected. Due to a slightly different DFB grating period, its emission wavelength is deviating from the other characterized lasers. Figure 1 compares the emission spectrum of this DFB QCL (0.9 mm short ridge-type QCL), recorded in the non-time resolved rapid scan mode (plotted in white with the right y-axis being the intensity scale) with the time-resolved emission spectrum recorded in step-scan mode (left y-axis is the time scale). The additional dimension facilitates a more detailed laser characterization, including information about the tuning rate and the actual temporal structure of the laser pulse. In this example the laser starts emitting near 1295 cm^{-1} (at t = 200 ns) and tunes towards lower wavenumbers (red shift) as time progresses. After 200 ns a mode-hop occurs which is again followed by a chirp to lower wavenumbers, a process which is repeated ~70 ns after initiation of the second mode. The observed mode hops of ~5 cm^{-1} and ~3 cm^{-1} are ascribed to different longitudinal modes from one side of the stop-band. Higher lateral order modes can be excluded because the narrow ridge (10 µm) with a lateral deposition of Si_3N_4 and Au provides a strong lateral-mode discrimination. Since the expected stop-band size is 1.6 cm^{-1}, a hop between the two modes on either side of this gap is not probably.

With the time-resolved measurement it could be determined that the laser maintained single wavelength emission during the whole pulse which was, however, split into three sub-pulses due to mode-hops. The non-time-resolved characterization does not reveal this important information, as the recorded envelope could equally correspond to full multimode operation during one pulse.

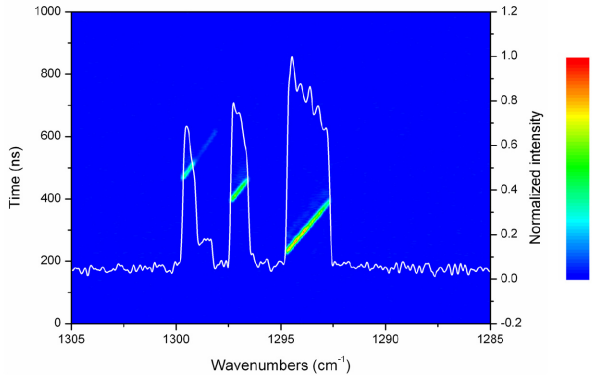

Fig. 1. Conventional non-time-resolved FT-IR measurement (white, solid line) of a short (0.9 mm) ridge-type QCL with an overlay of the corresponding step-scan measurement as contour plot. In addition to spectral and intensity domain data, time-resolved information is now provided. The laser repetition rate was 50 kHz and the driving current was 750 mA (8.33 kA/cm^2). Left axis shows time-domain data (pulses triggered at t = 200 ns) and right axis as well as color scale show normalized intensity data.

3.2 Time-resolved characterization

RCSE and short ridge DFB lasers had a similar cross section relevant for laser current density, i.e. laser current levels can directly be compared. Long ridge DFBs had a factor 3.2 larger cross-section which had to be considered. Thus, driving currents of the long DFB QCLs were adjusted a factor 3 higher, if not limited by the maximum laser driver current of 1800 mA. The cavity length L of DFB QCLs influences the spectral emission stability via the coupling strength κL [20]. With the effect that shorter cavities are more likely prone to laser instabilities, such as mode-hops (see Fig. 1). The spectral tuning characteristics of three

#200147 - $15.00 USD Received 29 Oct 2013; revised 2 Jan 2014; accepted 6 Jan 2014; published 30 Jan 2014

different laser configurations (please refer to Table 1) operated with a pulse length of 2 µs adjusted on the laser driver, were investigated, data are shown in Fig. 2. As expected, obtained results give evidence that the short ridge QCL exhibits inferior emission properties, e.g. in terms of spectral coverage compared to the long ridge version, indicated by a 2.5-4 times smaller spectral tuning range (see Fig. 2).

This observation is due to different gain levels at similar levels of current density. Especially, at short DFBs the provided gain is smaller because of higher mirror losses. This fact is confirmed by the respective threshold current densities. For the short DFB, a value of 3.8 kA/cm^2 was measured which is high compared to the RCSE (2.6 kA/cm^2) and the long DFB (2.5 kA/cm^2). Knowing the waveguide losses from simulations which are equal for the long and short ridge DFB, the extraction losses (mirror losses) can be calculated. They are 25.5 kA/cm^2 for the short DFB and 14.3 kA/cm^2 for the long DFB. This large deviation is in agreement with the expectations since mirror losses scale with 1/L and, furthermore, at over-coupled long devices the effect of the facets is reduced.

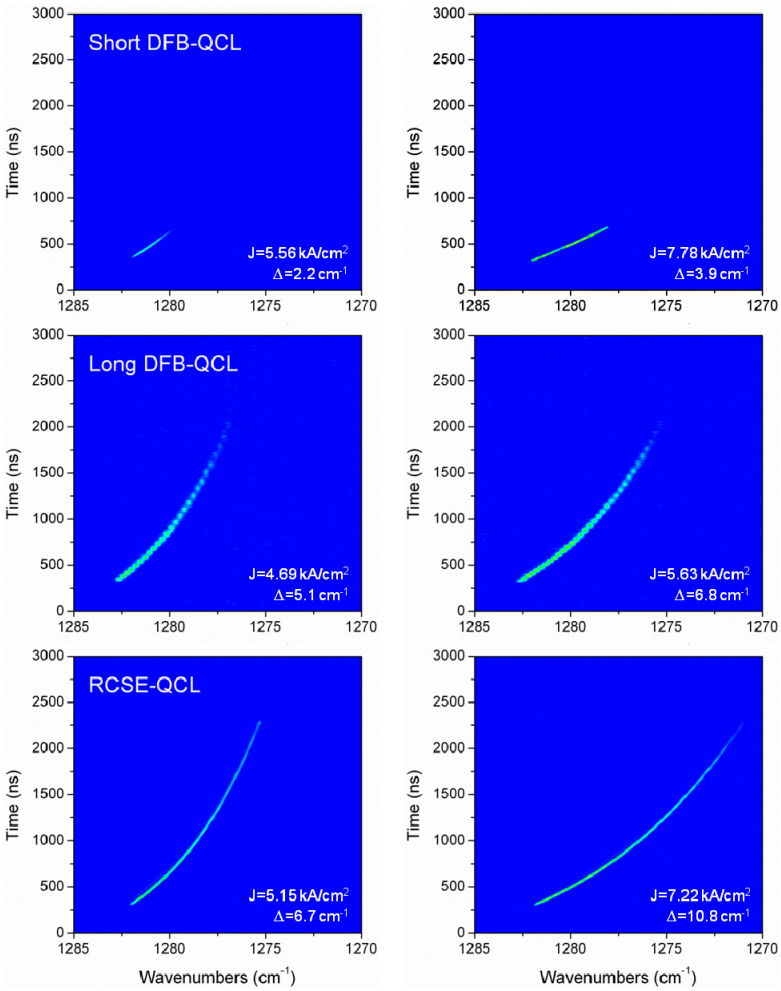

Fig. 2. Emission characteristics under different operation conditions (laser current densities J) for short DFB-QCLs (top), long DFB-QCLs (middle) and RCSE-QCLs (top). The laser repetition rate was 10 kHz and the pulse duration adjusted on the laser driver was 2 µs (pulses triggered at t = 250 ns). Δ-values represent the achieved spectral coverage for each device.

#200147 - $15.00 USD Received 29 Oct 2013; revised 2 Jan 2014; accepted 6 Jan 2014; published 30 Jan 2014

The RCSE device, although not over-coupled, exhibits a performance similar to the long DFB in terms of mode stability and threshold current density. This fact is ascribed to the absence of facets. Its stable emission expands over a spectral range even broader than that of the long ridge DFB. Based on the emission data of the RCSE QCL in Fig. 2 one can already anticipate the transition from pulsed operation to cw operation, which would be the case after thermal equilibrium is reached and the tuning rate becomes zero.

The above explanation of the experimental data in Fig. 2 assumes that the tuning rates solely depend on the laser current densities. However, different laser geometries could potentially influence the tuning rate and thereby the spectral coverage. In order to investigate this possible influence, Fig. 3 shows the experimentally determined tuning rates of the employed laser material as a function of laser current density (data obtained from a RCSE device). Furthermore, tuning rates that were observed for different device geometries (data from Fig. 2) are indicated in the graph. The obtained results are in general agreement regarding the dependence on the current density, thereby suggesting that the device geometry has a negligible influence on the tuning rates. This result is in accordance with the expectation, that spectral tuning due to Joule heating and device expansion is not influenced by device geometry. The latter becomes clear when considering that the ring cavity's circumference expands linearly with the temperature, such as the ridge-cavities.

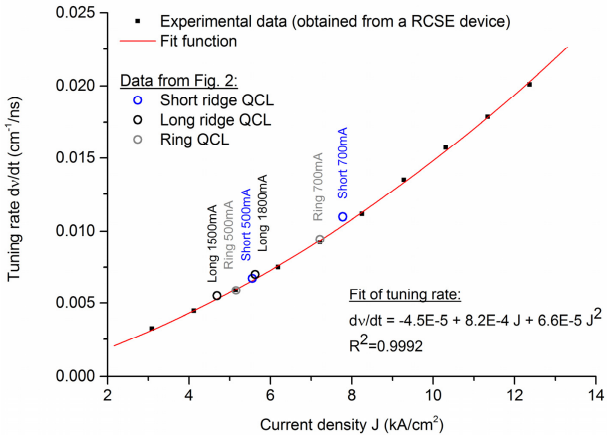

Fig. 3. Experimentally determined tuning rates of the employed laser material as a function of applied laser current densities (black squares, data obtained from a RCSE device). A polynomial fit of tuning rates and the corresponding coefficient of determination (R^2) is included for illustration. Tuning rates for different device geometries and current densities as extracted from data shown in Fig. 2 are indicated in the graph (colored circles).

Figure 4 shows the time-resolved tuning behavior of the RCSE laser for various driving currents. Although illustrative, the coloured intensity scale in the left graph is not ideal for a detailed quantitative evaluation. Therefore, a peak search function was applied to extract the course of the laser emission from the recorded data prior to data evaluation (Fig. 4, right). The truncation condition of the peak search function was chosen to be just above the noise level. A first order exponential decay fit ($A(I)\cdot e^{-\frac{t}{B(I)}} - c$) was found to be the optimum, physically plausible fit function. Here we summarize some exemplary data that can be retrieved from time-resolved step scan measurements. These data could e.g. serve as experimental basis for theoretical investigations of thermal effects, like shown in [21]. Step scan measurements of a selected RCSE Laser were performed for ten different laser currents starting from near lasing threshold at 300 mA towards 1200 mA, pulses started near t = 250 ns (Fig. 4). The roll-over current of the selected RCSE QCL was located at 1000 mA. Based on the time-resolved data the following characteristics of the laser can be deduced:

#200147 - $15.00 USD Received 29 Oct 2013; revised 2 Jan 2014; accepted 6 Jan 2014; published 30 Jan 2014

Starting wavenumber: The starting wavenumber, i.e. the spectral position where the laser starts to emit radiation is shifting towards lower wavenumbers (i.e. higher wavelengths) with increasing laser current. The overall shift observed between 300 mA and 1200 mA was 0.65 cm^{-1}. This effect can be explained by an incomplete thermal relaxation between consecutive laser pulses, hence the equilibrium temperature of the laser chip increases. Considering a temperature tuning rate of approximately −0.085 cm^{-1}/K [17] the observed shift would correspond to 7.6 K. A similar spectral shift will also appear if the duty cycle of the laser is increased, however, this was not in the focus of this work.

Chirp rate and maximum tuning time: The mean chirp rate increased from 3.2 * 10^{-3} cm^{-1}/ns at 300 mA laser current (= 3.09 kA/cm^2) to 1.8 * 10^{-2} cm^{-1}/ns at 1200 mA laser current (= 12.37 kA/cm^2) resulting in a total tuning range of approximately 1 cm^{-1} and 12.9 cm^{-1} respectively. Values for calculation of the mean chirp rate were taken from the first 250 ns of the pulse. The achieved maximum tuning time was similar for a certain range of injection currents (~2 µs for 400-700 mA). For higher laser currents the maximum tuning time decreased significantly which can be associated with the thermal losses that lead to a reduction of the lasing efficiency, i.e. heat-induced losses exceeded the provided gain towards the end of the pulse.

An intersection point of all fit functions (Fig. 4, right) was found, which can be interpreted as the point in time where the injection current pulse actually starts, but the laser is not emitting because the injection current has not yet reached lasing threshold. The time gap between intersection point and observing laser radiation certainly contains the rise time of the employed laser driver and detector. In terms of spectral information the intersection point can furthermore be seen as the wavenumber (respectively wavelength) where the laser would start to emit in case of a duty cycle close to 0%.

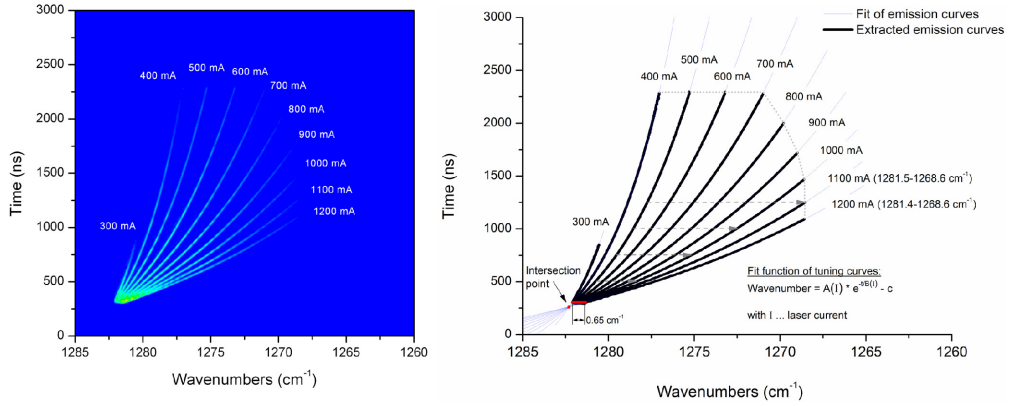

Fig. 4. (left) Results of time-resolved step-scan measurements of a selected RCSE-QCL at ten different laser currents (pulses triggered at t = 250 ns); (right) For clarity, spectral tuning curves were extracted with a peak search function and fitted with functions of the form $A(I)\cdot e^{-\frac{t}{B(I)}} - c$. At injection currents between 400 mA and 700 mA, the lasing time is basically limited by the pulse length that is 2 µs. At the other currents, the device stops lasing because the increasing losses exceed the heat-induced decreasing gain.

3.3 Ring-laser array

Arrays of surface emitting ring lasers have recently been presented as promising broadband laser sources for mid-IR spectroscopy [22]. In the present work, a compact 4x4 RCSE QC laser array was spectroscopically characterized by measuring the time-resolved emission behavior of three selected lasers of the array (see inset in Fig. 5). In contrast to the devices shown before that had an inner cavity radius of 150 µm, the ring cavities of the array had an inner radius of 190 µm, while the cavity width remained the same (10 µm). 2 µs long pulses were applied at a repetition rate of 20 kHz with a starting point of the pulses at t = 500 ns.

#200147 - $15.00 USD Received 29 Oct 2013; revised 2 Jan 2014; accepted 6 Jan 2014; published 30 Jan 2014

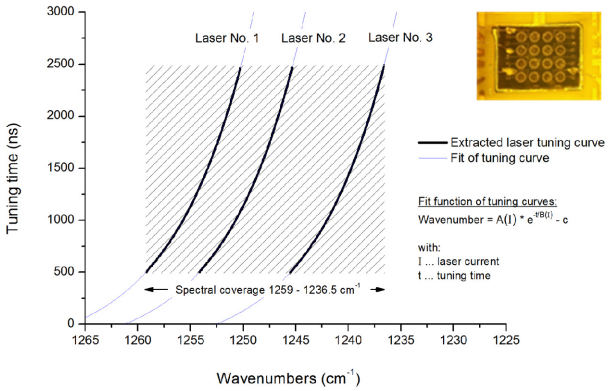

Fig. 5. Emission of three selected RCSE-QCLs that were part of an array of RCSE-QCLs (see inset) leading to a cumulative emission range of 22.5 cm^{-1} (pulses triggered at t = 500 ns).

The chosen lasers were designed to emit at 1245.5 cm^{-1}, 1254.1 cm^{-1} and 1259.2 cm^{-1}, respectively. The high chirp rate of the RCSE QC lasers allowed a cumulative tuning range of 22.5 cm^{-1} (see Fig. 5). For lasers no. 1 and no. 2 a wavenumber down-chirp of 8.5 cm^{-1} was achieved with a certain spectral overlap, whereas a down-chirp of somewhat more than 9 cm^{-1} was obtained with the third laser.

4. Conclusion and outlook

We have presented the step scan technique as a powerful tool for the characterization of mid-IR DFB QCLs. After the first application of the step-scan technique for time-resolved characterization of an external cavity QCL in [14] this paper concentrated the application for detailed comparison of DFB lasers with different resonator geometries, fabricated from the same laser material. The step scan approach is universally applicable to QC lasers and provides three dimensional information, comprising emission intensity as well as spectral and time domain. The only prerequisite for the technique is a reproducible laser signal. Device specific features, such as tuning rate, mode hops and the maximum effective emission time can be investigated by a single step-scan experiment. By the comparison of time- and spectrally resolved emission characteristics of 1st order DFB-QCLs and 2nd order RCSE-QCLs the advantage of facet-less devices could be demonstrated. From the obtained data it was concluded that RCSE-type QCLs are more stable than ridge-type devices in terms of less mode-hops and improved spectral coverage by injection current induced Joule heating. A maximum chirp rate of 1.8 * 10^{-2} cm^{-1}/ns was achieved with a single RCSE QCL chip leading to a spectral coverage of 12.9 cm^{-1}. Furthermore, selected lasers of a RCSE laser array were used to depict the illustrative visualization of the time evolution and time-dependent spectral overlap by step-scan measurements.

Time-resolved data are of high relevance for many spectroscopic applications of QCLs, e.g. in intra-pulse absorption spectroscopy. Step-scan FT-IR spectroscopy is a practicable technique that can provide this information with sufficient resolution both in the spectral and time domain.

Acknowledgments

We thank our collaborators at Princeton University (Group of C. Gmachl) for providing the QCL material, L. Palliyaguru for experimental assistance and W. Tomischko for assistance in all electronic related issues (both Vienna University of Technology). Financial support was provided from the Austrian Science Fund project NEXTLITE (FWF F4909-N23) and the Austrian research funding association (FFG) under the scope of the COMET program within the research network “Process Analytical Chemistry (PAC)” (contract #825340).